Acta Cryst. (1995). B**51**, 468–482

Diffraction Studies of Crystals at Low Temperatures – Crystallography Below 77 K

BY FINN KREBS LARSEN

Department of Chemistry, Aarhus University, DK-8000 Aarhus C, Denmark

(*Received* 25 *June* 1994; *accepted* 24 *March* 1995)

Abstract

Presently two well established cooling techniques prevail in crystallography: cold nitrogen-gas-stream cooling, which allows a minimum temperature close to the boiling point of nitrogen, 77 K, and closed-cycle helium refrigeration, which can reach temperatures even below 10 K. Some advantages and disadvantages of the cooling techniques are contrasted and recent technical developments are presented, in particular regarding data collection below 77 K. Three examples of charge-density studies are used to illustrate improvements in results obtained in small moiety crystallography by collecting data at very low temperatures. $H_8Si_8O_{12}$ is a case showing how temperature influences radiation damage. $KTiO(PO_4)$ is a case of a non-centrosymmetric structure where anharmonic motion was reduced and the charge density was established more convincingly. $(ND_4)_2Cu(SO_4)_2.6D_2O$ is a case of a combined X-ray and neutron (X/N) diffraction study of a Jahn–Teller distorted Cu^{II} compound in a minimum energy conformation.

1. Introduction

The advantages of collecting diffraction data at low temperatures are widely recognized among crystallographers, but perhaps for different reasons and with different emphasis. Protein crystallographers enjoy the fact that radiation damage is greatly reduced at low temperature, so crystals last longer in the beam. Small moiety crystallographers probably first think of the improvement in the precision and the accuracy of their studies, which may be achieved by conducting the data collection at low temperature. Small moiety crystallographers furthermore have developed methods of growing crystals of low-melting compounds by cooling and also use temperature as a very illuminating parameter in examining and displaying physical and chemical properties of solid-state materials.

Most crystallographic laboratories exploit the advantages of cryocrystallography and modern diffractometers are supplied with cooling equipment, often in the form of a liquid-nitrogen gas cooler. Thus, many crystallographers are accustomed to working with cooling equipment or at least have easy access to collecting data at temperatures approaching 77 K, the boiling point of liquid nitrogen. The present paper will primarily deal with the further advantages and also problems of single crystal crystallography below 77 K, and the emphasis will be on the improvements of structural results obtained by collecting data at very low temperature.

2. How cold?

Naturally, the question about at which temperature the crystallographic experiment ideally should be conducted depends on the problem one is tackling, and for this reason the greatest flexibility is obtained with diffraction equipment capable of collecting data at any temperature from room temperature down to a few degrees K. The following considerations may help decide which temperature capability to aim for.

2.1. *Phase transition studies*

Low-temperature crystallographic studies have been absolutely essential for the detailed understanding of the changes in physical properties of compounds going through solid-state phase transitions. Certainly, many interesting phase transitions do occur above liquid nitrogen temperature – a notable example is the transition to the superconducting state of the best high T_c superconductors. However, many occur at temperatures much lower than 77 K. Also, for this reason it is very desirable and often necessary that the diffractometer has a temperature capability extending to close to the absolute zero point. One-dimensional organic conductors can be used as an example. These materials exhibit electronic properties which change with temperature and which cannot be fully explained without the knowledge of the corresponding lattice changes or distortions. The first communication on the metal-like one-dimensional conductivity in an organic compound was for the donor–acceptor complex tetrathiofulvalene–tetracyano-*para*-quinodimethane [TTF–TCNQ; σ_{max}(obs) = 1.47 x 10^4 Ω^{-1} cm^{-1} at 66 K (Ferraris, Cowan, Walatka & Perlstein, 1973)]. It spurred a hectic activity in the field which lasted through the 70s and early 80s. Hundreds of low-dimensional organic conductors were synthesized and characterized and it was realized that these materials, which exhibit different forms of columnar stacking of flat molecules, show a wealth of interesting crystallographic features which had to be described and understood at the atomic level before properties could be accounted for and new compounds engineered.

After an interlude of much focusing on the high-temperature superconductors there are signs that interest in one-dimensional organic conductors is again starting to flourish. It may therefore be appropriate to refocus on TTF–TCNQ, which has remained the protype one-dimensional organic conductor. Study of the diffuse scattering (Comés, 1977) showed a progressive coupling between the charge-density waves on different molecular stacks when lowering the temperature. At 54 K a sinusoidal modulation of the lattice results from this coupling and is manifested by the appearance of satellite reflections around the main Bragg peaks from the undistorted high-temperature crystal. TTF–TCNQ undergoes a series of transitions at 54, 49 and 38 K. Much work, reviewed by Filhol (1994), has established that first TCNQ stacks are Peierls distorted by a transition at 54 K, then also the TTF stacks undergo displacement at 49 K, and finally a lock-in of the distortion wave occurs at 38 K. In spite of drastic changes of physical properties at the phase transition, from metallic conduction above 54 K, to semiconductivity below that temperature, the corresponding systematic atomic displacements are small, sometimes a fraction of the thermal atomic displacement. Consequently, satellite intensities are typically not more than 10^{-4} times the intensities of the main reflections. Coppens *et al.* (1987) used synchrotron radiation to collect sufficient satellite reflections for a study of TTF–TCNQ at 15 K. The incommensurately modulated structure was described in the five-dimensional superspace group $P^{P2_1/c}_{cmm}$. Bouveret & Megtert (1989) reported another investigation of the lowest temperature-modulated phase of TTF–TCNQ based on an extended set of 621 satellite reflections measured at 13 K on a diffractometer equipped with a rotating anode. Further, very accurate crystallographic studies are necessary for the proper description of the full progression of phase transitions in TTF–TCNQ. Phase transitions in magnetic materials have also attracted much attention. Intricate and beautiful spin distributions have been revealed and, for example, the antiferromagnetic magnetic spiral found in many of the rare earth metals undergo a number of transitions at temperatures far below 77 K (Bohr, 1991).

Sometimes it is difficult to disentangle in a crystallographic study the results of molecular disorder. In such cases, data collected at different temperatures may be of help in obtaining structural information by discerning between statistical and dynamic disorder. Thus, some structural information is only obtainable by having low-temperature data available. Another aspect is the improvement of precision and accuracy of structural information by collecting data at low temperatures. The remainder of the paper puts emphasis on this point and concentrates on the single crystal experiment, which in that respect is superior to the powder diffraction experiment. It should be mentioned though that low-temperature powder diffraction studies are definitely experimentally less involved. Data collection in the mK range can be realized rather easily for powdered samples in contrast to the single crystal experiment at such temperatures, and so much interesting information is obtained by very low-temperature powder diffraction studies (Hathaway & Hewat, 1984).

2.2. *Radiation damage*

Both for macromolecular and small moiety crystals, extensive experience has shown how radiation damage and other decay can be dramatically reduced if a crystal is kept near liquid nitrogen temperature during data collection. Recent development in gas cooling cryocrystallography has led to huge strides in the advancement of the study of biological macromolecules, mainly because of the reduction in crystal radiation damage (Hope, 1988), and for instance has made feasible data collection from ribosomal particles (Hope *et al.*, 1989). Presumably the production of free radicals responsible for radiation damage continues at the low temperature, but the radicals are trapped. If an irradiated crystal prone to radiation damage warms up enough to allow the radicals to diffuse, they will do their damage. Because diffusion is involved, sizable radiation damage may still occur at 100 K for some small moiety crystals, so reducing the temperature even further may be advantageous. Unfortunately, it is not always possible to completely prevent radiation damage even at quite low temperatures. Later in the text an example will be given of a case – data collection for a charge-density study of silasesquioxane, $H_8Si_8O_{12}$ – where some radiation damage evidently still occurred at 9 K.

2.3. *Charge-density studies*

A chemical crystallographer wanting to experimentally determine the electron-density distribution of a molecule, to a detail which may allow calculation of electrostatic potentials to evaluate molecular reactivity and possibly also a topological analysis of the charge density, would be advised to collect data at very low temperature. In that way all the benefits which come from the ensuing decrease of atomic thermal motion – reduced thermal diffuse scattering (TDS), improved resolution and less anharmonicity – can be reaped.

2.3.1. *TDS.* The intensity of X-rays scattered by a crystal is the sum of the elastically scattered Bragg intensity and the inelastic TDS. The TDS from the optic modes of lattice vibrations tends to give a contribution, which is constant across the diffraction peak, and so is corrected for during data integration by normal background subtraction. However, the contribution of the acoustic modes peaks at the Bragg position and should be corrected for in a separate calculation, which is complicated because it depends on collimation and scan type, and can only be performed if the elastic constants of the crystal are known. Coppens & Vos (1971) made

an analysis of the temperature dependence of mean-square displacements for a number of frequencies of a vibrator with the mass of the cyanuric acid molecule. They concluded that all modes above *ca* 100 cm^{-1} are practically in their ground state at liquid nitrogen temperature and so will not contribute to TDS. For such modes, the advantage of decreasing the temperature below 77 K is minimal. However, for typical molecular crystals the frequencies of many lattice modes are below 100 cm^{-1} and it is advantageous to further reduce the temperature in order to de-excite as completely as possible most of the low-frequency lattice modes. For data collected around 10 K, TDS is usually deemed insignificant.

2.3.2. *Resolution.* Data collection temperature influences the observed electron density $\rho_T(\mathbf{r})$,

$$\rho_T(\mathbf{r}) = (1/V)\sum_{\mathbf{H}} F_T^o(\mathbf{H})\exp(-2\pi i\mathbf{H}.\mathbf{r}),$$

through its influence on the structure factors $F_T^o(\mathbf{H})$ in a way which may be illustrated by the expression for the model structure factor, $F_T^c(\mathbf{H}) \simeq F_T^o(\mathbf{H})$. For a structure composed of N atoms at positions $\mathbf{r_j}$ in the asymmetric unit

$$F_T^c(\mathbf{H}) = \sum_{j=1}^{N} f_j(\mathbf{H})T_{T,j}(\mathbf{H})\exp(2\pi i\mathbf{H}.\mathbf{r_j}).$$

Structure factors fall off with increasing scattering angle because of the combined effect of similar functional shapes of the atomic scattering factors $f_j(\mathbf{H})$ and temperature factors $T_{Tj}(\mathbf{H})$. In the approximation of isotropic atomic thermal vibration

$$T_{T,j}(\mathbf{H}) = \exp\left(-8\pi^2 < u_{T,j}^2 > \sin^2\theta/\lambda^2\right),$$

where $< u_{T,j}^2 >$ is the mean-square displacement of atom j at temperature T. It may be expected that parameters describing thermal motion tend to correlate with density parameters. For many compounds $< u_{T,j}^2 >$ is proportional to T above 77 K. By lowering the temperature of the sample crystal, the atomic temperature factors increase and more reflections gain intensity to become significant. In this case it becomes meaningful to collect data to higher values of $\sin\theta/\lambda$. Hope (1988) estimated that for a typical macromolecule the highest resolution will improve from 3 Å at 300 K to 2 Å at 100 K. Larsen (1991) illustrated the improvement in resolution obtained by cooling by calculating for a typical small moiety crystal the enhancement factor which applies to the intensity at different $\sin\theta/\lambda$ values. At $\sin\theta/\lambda$ = 1.0 $Å^{-1}$, lowering the temperature from 300 to 100 K gives a factor of 150 in intensity enhancement and a further factor of 5 by going to 10 K. At $\sin\theta/\lambda$ = 1.3 $Å^{-1}$ the factors are $\sim$ 500 on going from 300 to 100 K and a further factor of approximately 10 by going to 10 K. By lowering the temperature, high-order data become available, which makes precise electron-density studies feasible for many crystal structures. By lowering the temperature to 100 K, usually enough significant reflections can be measured out to $\sin\theta/\lambda$ = 1.0 $Å^{-1}$ that there will be approximately five observations per parameter for the least-squares refinement of a multipole model of the atomic charge-density distributions, and it has been amply proved that convincing electron-density studies can be performed with 100 K data. The precision of the studies though may be improved by lowering the temperature to *ca* 10 K, which will, for a complete set of data measured to a $\sin\theta/\lambda$ value of 1.3 $Å^{-1}$, give approximately ten observations per parameter.

2.3.3. *Anharmonicity.* The assumption usually applied in the modelling of the atomic temperature factor is that forces between pairs of atoms in a crystal are proportional to their relative displacements. This is the harmonic approximation. Under this assumption, the atomic thermal motion can be described by six parameters in the general case. In reality, many atoms sit in shallow asymmetrical potential wells resulting in anharmonic motion, which can also be modelled fairly well, but at the expense of introducing many extra parameters in the description of the temperature factors. It should be noted that anharmonic effects become more pronounced at higher temperatures. Unfortunately, this means that more thermal parameters are needed, when fewer significant observations are available for refinement. Cooling improves the situation in two ways. The number of significant reflections is increased and at the same time many of the anharmonic parameters become insignificant, which may allow a simplification of the model and thus a reduction in the number of thermal parameters. For this reason, deconvolution of thermal motion and electron-density contributions to the structure factor become less of a problem at low temperature, and the lower the temperature the better. An added advantage is that the displacement parameters become less temperature dependent at the very lowest temperatures. The constancy of the experimental temperature is less critical at 10 than at 100 K. Consideration of anharmonic effects will be given for the examples of charge-density studies on $KTiOPO_4$ and $(ND_4)_2Cu(SO_4)_2.6D_2O$ presented later in the text.

In the next paragraph the most successful cooling methods are reviewed. First, and briefly, the gas-stream cooling technique which can give data collection temperatures down to a little less than 100 K, and then the helium cryorefrigerator cooling technique which can bring the temperature even below 10 K.

3. Cooling techniques and apparatus

A variety of cooling techniques have been used to study the low-temperature properties of materials and

numerous types of cooling equipment have been built. An extensive survey was given by Rudman (1976) in his book '*Low-Temperature X-ray Diffraction. Apparatus and Techniques*'. Much useful information can also be found in the American Crystallographic Association publication of lecture notes from a Low-Temperature X-ray Diffraction Tutorial held at a meeting in Asilomar, California (Rudman, Hope, Stevens & Petsko, 1977) and a review article by Veith & Frank (1988). Some more recent developments are covered in a contribution by Larsen (1991) on '*Necessity and Pitfalls of Low-Temperature Measurements*', which appeared in the Proceedings of a NATO Advanced Study Institute on the Application of Charge Density Research to Chemistry and Drug Design, and one by Luger (1993) from a Colloquium at Humboldt University in Berlin on the occasion of '80 *Years X-ray Diffraction*'.

For accurate crystallographic studies at low temperatures, two methods in particular for cooling the sample have been developed to great sophistication:

(1) The gas-stream method in which a stream of cold gas is directed at the sample.

(2) The conduction method in which the crystal is cooled through contact with a good thermal conductor, which is part of a cooling unit such as a coolant reservoir or a Joule–Thomson expansion device.

General principles in the construction of the two types of devices will be described.

3.1. *Gas-stream cooling*

Usually for economic reasons nitrogen gas is used and liquid nitrogen is used as the coolant. Nitrogen gas is boiled off liquid nitrogen in a Dewar vessel and subsequently by means of pumps and valves turned into a constant flow of nitrogen gas, which is recooled by heat exchange with the liquid nitrogen before escaping through a delivery nozzle. The concept is thus quite simple and scores of modifications of gas-stream cooling equipment have been designed.

A very convenient feature of the gas-cooling technique is that the sample crystal can be seen even when cooled. Mounting and centring of the crystal on the diffractometer is straightforward and also the interesting possibility of growing single crystals from liquids contained in a capillary mounted at the sample position is feasible, while it is much harder in the case of conduction cooling. However, the nozzle construction and its positioning as close to the sample crystal as possible is tricky. This is essential for reaching the lowest practical temperature and also to prevent frosting. The principle of making an envelope of warm gas in a laminar flow with the cold gas usually pretty well takes care of the frosting problem, but even so it is often deemed necessary to surround the entire diffractometer with a dry-box. This upsets some of the advantages of the open construction of the gas-cooling equipment. Another difficulty of this cooling method is to determine routinely the absolute value of the sample temperature. The temperature is usually monitored by a thermocouple, which is positioned in the cold-gas stream near the mouth of the nozzle. This opening can only be brought within a few millimetres from the sample crystal in order not to interfere with the incoming and diffracted X-ray beams. Therefore, there is bound to be a temperature gradient between the tip of the thermocouple and the crystal. Experience from the literature shows that the sample temperature can be easily misjudged, and this can be a highly disturbing effect when results are compared or worse if one wants to refine simultaneously diffraction data from independent experiments as in X/N studies.

3.2. *Conduction cooling*

The sample crystal is mounted on a cooling block through which the coolant passes. In order to prevent condensation, the crystal and the cold parts of the cryostat have to be enclosed in a vacuum. For X-ray diffraction, an outer shroud of beryllium is often used. Sometimes extra shrouds are introduced inside to reduce heating the crystal by radiation. The wall of inner confinements is kept in thermal contact with the cooling block, which ensures that the crystal is part of the temperature equilibrium. The crystal temperature is measured very reliably by a sensor embedded in the cooling block.

3.3. *Joule–Thomson cooling*

Cooling with nitrogen gas can achieve temperatures even below 77 K. A vacuum-assisted Joule–Thomson refrigerator (manufactured by MMR Technologies Inc., CA 94043, USA) provides cooling to 68 K. Refrigeration is obtained by expanding high-pressure nitrogen gas through small capillaries in a laminated glass refrigerator. The gas cools upon expansion and liquefied nitrogen is produced inside the refrigerator, collected in a liquid reservoir, and used to cool the refrigerator cooling block. The boiling point of the liquid is determined by the vapour pressure of the nitrogen gas in the reservoir. Temperatures below that of liquid nitrogen at atmospheric pressure (77 K) are achieved using a vacuum pump to evacuate gas through the exhaust channels of the liquid reservoir of the refrigerator. The cooling unit is small and compact and it should be possible to fit it onto most diffractometers.

3.4. *Flow-cryostats*

Some flow-cryostats operate with the coolant in the form of either liquid nitrogen or liquid helium being pumped through the cooling block. Consumption of cryogen is comparable to that of open gas-flow systems, but for a flow-cryostat recuperation of spent cryogen gas is relatively straightforward, which makes it economically more feasible to use liquid helium. This

opens up the possibility of cooling to temperatures even below 10 K. Flow-cryostats using liquid coolant can be made rather compact and therefore can be fitted onto four-circle diffractometers (Coppens *et al.*, 1974; Zeyen, Chagnon, Disdier & Morin, 1984), and even chi-geometry diffractometers (Albertsson, Oskarsson & Ståhl, 1979). They have generally proven to be difficult to work with and in spite of some notable successes, they seem largely to have been abandoned in accurate X-ray diffraction work. The major problem has been to position the stiff vacuum-jacketed lines which are used to bring the cryogen from the supply Dewar to the flow-cryostat. The cryogen lines often impair the diffractometer movements. The flow-cryostat designs used for single crystal diffraction all seem to incorporate rotating seals separating the coolant at cryogenic temperatures from the atmosphere at ambient temperature. It has turned out to be an exceedingly difficult problem to make these seals tight without placing excessive force on the mechanical parts of the diffractometer. The slightest leak in seals of this type will ice it up and impair the rotational movement of the crystal.

Helium flow-cryostats have a consumption of at least 0.5 l h^{-1} of liquid helium when maintaining the sample temperature at 10 K. Liquid helium is quite expensive and often not easily accessible. Therefore, even if some of the major obstacles in the use of flow-cryostats can be removed, the inconvenience of handling and the considerable expense of buying liquid helium will still exist and make helium flow-cryostats unattractive for general crystallographic work. Fortunately, there is an alternative cooling device which allows crystallography at very low temperatures. Joule–Thomson coolers in the form of closed-cycle helium refrigerators which use no cryogen have been developed into compact reliable devices capable of maintaining the temperature of a sample crystal at 10 K.

3.5. *Closed-cycle helium refrigerators*

In the mid-seventies a new development in the pursuit of crystallographic studies at temperatures below 77 K began when a closed-cycle helium refrigerator was first adapted to a diffractometer. The closed-cycle helium refrigerator comprises a compressor unit and an expander module connected with flexible gas lines. The compressor pressurizes the helium gas for the expander where refrigeration is accomplished by adiabatic expansion of the helium. Fig. 1 shows a simplified diagram of this type of refrigerator, a Displex two-stage Gifford–McMahon-type expander module (manufactured by APD, Cryogenics Inc., Allentown, PA 18103, USA). The valve motor turns the valve disc, which determines the operating cycle of gas intake and exhaust. High-pressure helium admitted by the rotating valve disc during the intake period flows through the slack cap and into the regenerators. The regenerators, cooled during the previous exhaust stroke, cool the incoming gas as it flows through. Gas flowing through raises the slack cap and lifts the displacer, creating expansion space at the heat stations for gas that has passed through the regenerator. Also as the displacer lifts, gas above the slack cap is partially compressed and pushed through the orifice into the surge volume. Before the displacer reaches the valve stem, the valve closes. Compression of gas above the slack cap decelerates and stops the displacer before it can collide with the valve stem. When the valve opens to exhaust, high-pressure gas at the heat stations is free to expand and thereby refrigerate them. The exhausting gas also cools the regenerators. As the pressure drops, partially compressed gas bleeds from the surge volume, pushes the slack cap and displacer towards the heat stations, forces exhaust, and positions the displacer for the next cycle. After *ca* 1 h of operating time, a two-stage expander working at full capacity will have decreased the temperature to less than 10 K at the second station.

4. Development in the cryocooler technique

Three-stage closed-cycle helium cryocoolers capable of reaching 3.6 K are commercially available, but, unfortunately, they are still rather bulky, heavy and expensive, and not ideal for use in crystallographic studies. However, it seems that also the two-stage Gifford–McMahon cryocooler has potential for reaching working temperatures in the vicinity of the boiling point of helium. The conventional two-stage cryocooler usually has densely packed fine-meshed copper nets in the first stage regenerator. In the second stage regenerator lead in the form

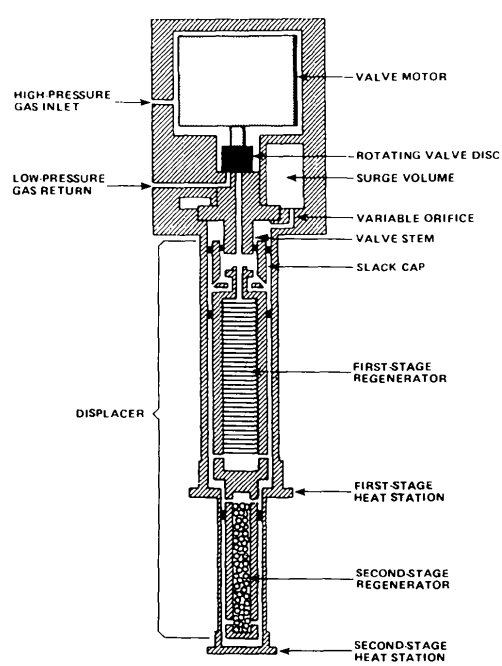

Fig. 1. Schematic diagram of a two-stage Displex expander module (manufactured by APD, Cryogenics Inc.).

of lead spheres (0.2–0.3 mm in diameter) is preferred because of its high heat capacity below 80 K. The specific heat for lead, however, decreases rapidly with decreasing temperature, making the refrigeration power and efficiency around 10 K so small that the lowest practically attainable temperature is limited to $\sim$ 8 K. Materials have been found and explored, notably Er_3Ni, which have much higher heat capacities per unit volume than lead below 10 K (Sahashi *et al.*, 1989). In a non-magnetic substance, such as lead, only the lattice vibrations and the conduction electrons contribute to the specific heat. For magnetic materials the spin interactions may contribute considerably to the specific heat near the magnetic phase transition. Er_3Ni has a complicated spin configuration around 7 K, resulting in a considerable volumetric specific heat right down to 5 K, which is higher than that of lead below 15 K and comparable with it at higher temperatures. Kuriyama *et al.* (1989) reported reaching a lowest temperature of 4.5 K using Er_3Ni as second-stage regenerator material in a two-stage Gifford–McMahon refrigerator. The refrigeration capacity below 10 K at the second stage is approximately 2 W better for Er_3Ni than for lead. Nb_3Sn is another material which is being used successfully in the second stage. Producing small spheres of the new materials is a technical challenge and expensive. Mixing in lead spheres makes the construction more affordable while still giving improved performance. Two-stage expander modules which offer 6.5 K are now commercially available.

Two-stage Gifford–McMahon refrigerators have mainly been developed for stationary use in applications where weight and size of equipment are of minor importance. Typically, the commercially available two-stage refrigerators weigh around 5 kg and have an overall length of *ca* 40 cm. Consequently, the first applications of such cooling devices for low-temperature single crystal diffraction work have been at physics research centres where traditionally, large and sturdy four-circle diffractometers are part of the equipment. More and more university laboratories choose to buy large four-circle diffractometers (*e.g.* the Huber diffractometer with the big Eulerian cradle, type No. 512) in order to facilitate mounting of auxiliary equipment such as two-stage refrigerators. The finding of more efficient regenerator materials will hopefully result in the miniaturization of two-stage refrigerators to a degree that they may be used with just a few modifications of existing diffractometers.

5. Mounting cryocoolers

A huge advantage of the closed-cycle helium Gifford–McMahon cryocoolers is that they use no cryogen, thereby avoiding the encumbrances associated with the flow of liquid nitrogen or helium through pipes, jacketed flexible tubing and rotatable joints. The relatively small expander unit with the cold stations is separated, but connected to the heavy compressor with flexible tubes which transport the pressurized room-temperature helium gas.

Cooling of the crystal must be achieved by conductance when using cryocoolers for low-temperature crystallography. Furthermore, the crystal and the cold stations must be surrounded by a vacuum in order to prevent frosting. Therefore, mounting a cryocooler say on a four-circle diffractometer presents rather complicated problems which have resulted in intricate designs. One solution (Samson, Goldish & Dick, 1980) involved allowing the crystal to rotate relative to the cold station of the cryocooler and let the thermal conduction occur through a flexible, very high purity copper cable. The construction has the attractive feature that the incident and diffracted X-ray beam cuts through narrow kapton-foil covered slits in the spherical vacuum shroud, *i.e.* absorption by the X-ray windows is small and identical for all reflections. However, mechanically it is a very difficult and expensive solution, which includes different types of dynamic vacuum seals between moving parts separating the vacuum from the exterior. The seals have to be adjusted well as a compromise between excessive friction for the moving parts and leakage into the vacuum. In other solutions (Henriksen, Larsen & Rasmussen, 1986; Archer & Lehmann, 1986) the crystal is mounted rigidly on the 10 K cold station, which means that the cryocooler must follow all the crystal movements and rotating seals may be avoided completely. Conceptionally, the mount is just a giant goniometer head without arcs and the cryocooler with vacuum shroud is an integral part hereof. A two-stage Displex cryocooler mounted on a Huber diffractometer in a Henriksen, Larsen & Rasmussen (1986) centring device is shown in Fig. 2. The lower part of the vacuum shroud is a beryllium cryostat chamber which serves as an X-ray window. Absorption in the cylinder wall is easily calculated but relies on uniform wall thickness. There will also be powder scattering from the beryllium cylinder walls, but by having a cylinder of accurate radius it is possible to collimate the X-ray beam so that powder scattering from the off-centre beryllium walls will not reach the counter.

Beryllium has excellent properties for this application, low X-ray absorption, vacuum tightness and good mechanical strength, although it is somewhat fragile at the wall thicknesses desired for low X-ray absorption. Regrettably, beryllium is a toxic substance which can be machined only under extreme precautions. Therefore, the choice of shapes and sizes of cryostat chambers made of beryllium is restricted and they are quite expensive. Recently, cryostat chambers made of carboneous composite material coated with a thin layer of aluminium (Coppens, Coppens & Lee, 1993; manufactured by Anholt Technologies, Inc., Delaware 19711, USA) have become an alternative to beryllium chambers as

a combined vacuum shroud and X-ray window. Carboneous composite material has X-ray absorption characteristics rivalling those of beryllium, and chambers can be made in different shapes and sizes at a cost significantly lower than a beryllium analogue. Furthermore, the composite chambers are less fragile and easier to handle and thus offer an interesting alternative to beryllium chambers.

Advances in area detector technology are presently opening possibilities for the increased speed, sensitivity and resolution of diffraction studies. However, the use of imaging plates or similar devices for experiments using conduction cooling equipment demands changes in the conventional construction of the target crystal confinement and in the positioning of the beam stop. When using a point detector, such as a scintillation detector, powder lines stemming from vacuum chamber and radiation shields may be effectively avoided by positioning a collimator of small diameter in front of the detector. In that case, a beam stop is not strictly necessary, except for health and safety reasons. Using an area detector the only way to avoid recording powder lines and excessive background intensity is to position the beam stop and stray-radiation shielding close to the crystal, *i.e.* inside the cryostat chamber and radiation shield. A solution to that problem has been designed and elegantly constructed by Darovsky, Bolotovsky & Coppens (1994) using a movable beam stop, which is fastened inside the confinement to a ball bearing concentric with the cylindrical vacuum shroud. A strong permanent magnet is also fastened to the beam stop, which can then be positioned from outside the vacuum shroud through magnetic coupling to an outer strong magnet.

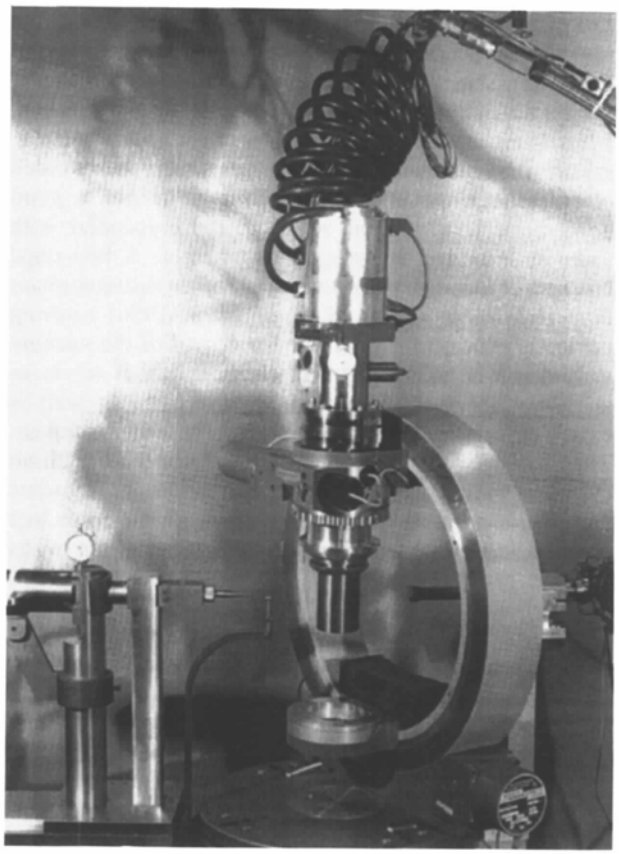

Fig. 2. Two-stage Displex DE202 cryocooler mounted in a Henriksen, Larsen & Rasmussen (1986) centring device on the φ bearing of a Huber 512 four-circle diffractometer. Helium gas lines and electrical connection are supported from the ceiling by a swinging link suspension.

6. Low-temperature diffraction studies

Some case studies taken from personal experience with crystallography below 77 K will be used to illustrate improvements in results obtained from small moiety crystallography by collecting data at very low temperatures.

6.1. $H_8Si_8O_{12}$: *a case of radiation damage proceeding at* 9 K

Cooling the crystal gives the added bonus that radiation damage is reduced. Generally, the radiation damage reduces the lower the temperature. However, even when cooling to temperatures around 10 K, radiation damage may still persist without being very obvious.

The study of the silasesquioxane $H_8Si_8O_{12}$ can be mentioned as an example. Fig. 3 is a drawing of the structure. Sphero-silesquioxanes are cage-like molecules composed of several RSiO$_{1.5}$ units. The hydrogen-substituted species is oxygen- and moisture-sensitive, as well as intrinsically unstable due to incipient nucleophilic attack of O on Si. The structural properties are largely determined from the combination of flexible Si—O—Si angles and non-flexible O—Si—O angles in the molecule. Auf der Heyde, Bürgi, Bürgy &

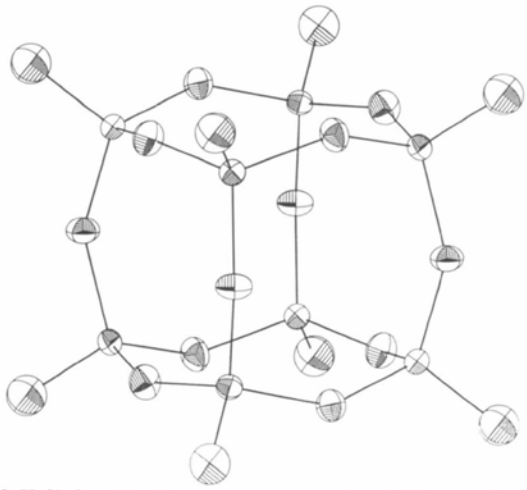

Fig. 3. $H_8Si_8O_{12}$. The silasesquioxane molecule at 9 K drawn with atoms at the 90% probability level.

Törnroos (1991) published structural results based on 100 K Ag $K\alpha$ X-ray data. A precise geometry was established, and it was even possible to infer reasons why the almost cubic molecule has small deviations from $m\bar{3}m$ symmetry. The molecular packing namely results in four relatively short Si—O contacts between pairs of molecules – the site of incipient nucleophilic attack of O on Si. The thermal motion was analysed and convincingly indicated that $H_8Si_8O_{12}$ has major deviations from rigid-body behaviour in spite of the low temperature. During the 100 K data collection it was observed that high-order standard reflections lost on average 12% of their intensity in 5 d, which was taken to indicate radiation damage. It was therefore deemed necessary to obtain an accurate and detailed charge-density distribution that new data should be collected at the lowest possible temperature in order to eradicate or at least diminish further the radiation damage. Seiler (1992) has demonstrated that the initial effect of radiation damage in a crystal is to increase the number of defects and the static disorder in a way which may simulate an increase in the sample temperature. He showed that radiation damage thus gives a scattering angle-dependent reduction in intensity. We collected Mo $K\alpha$ radiation data at 9 K and took precautions to recognize and monitor radiation damage by including high-order as well as low-order reflections in the group of standards.

The virtual increase in the sample temperature which is caused by radiation damage should also reflect itself as changes in the cell dimensions proportional to the irradiation time. Data collection for $H_8Si_8O_{12}$ was set up to include this aspect as well. The orientation matrix was checked regularly and cell dimensions were redetermined nine times during the 55 days the crystal was kept cold. The actual sample temperature, as measured in the crystal mount inside the vacuum chamber of the Displex cryocooler, slowly rose from 8.2 (1) to 10.2 (1) K during that period. This small temperature rise should hardly influence the magnitude of the cell dimensions, particularly at this very low temperature. Nevertheless, cell dimensions grew significantly larger. They increased proportionally with time, as shown in Fig. 4, which we interpret to be a result of radiation damage. Cell dimensions at 100 K for $H_8Si_8O_{12}$ were reported by Auf der Heyde, Bürgi, Bürgy & Törnroos (1991) to have the values $a = b = 9.047\,(1)$ and $c = 15.162\,(4)$ Å. Starting values for the cell parameters at 8.2 K were $a = b = 9.018\,(1)$ and $c = 15.113\,(7)$ Å, and at 10.2 K, at the termination of the experiment, they had increased to the values $a = b = 9.029\,(1)$ and $c = 15.123\,(7)$ Å. Assuming that the cell dimensions increase linearly with temperature between 8 and 100 K, the radiation damage causes a nominal rise in sample temperature of 35° in 55 d.

According to Seiler's (1992) suggestion, the concomitant radiation-damage-induced reduction of intensity is predicted to be a function of time, which may be described by a factor $\exp[-2\Delta B(t)\sin^2\theta/\lambda^2]$. Refinements of the 100 K data corrected for the intensity decay of standard reflections showed the equivalent isotropic temperature factor parameters $B_{eq}(Si) = 0.80\,(1)$ and $B_{eq}(O) = 1.27\,(1)$ Å^2. Relative to this, the unscaled 9 K data thermal parameters were found to have been reduced by a factor of 0.45 to the values $B_{eq}(Si) = 0.36\,(1)$ and $B_{eq}(O) = 0.56\,(1)$ Å^2. Assuming that B_{eq} is proportional to T even below 100 K, the virtual temperature of 43 K accounts surprisingly well for the factor $0.45 \simeq 43/100$ K, as can be seen in Fig. 5, which shows the values of the present study plotted at the virtual temperature of 43 K, while those of the previous

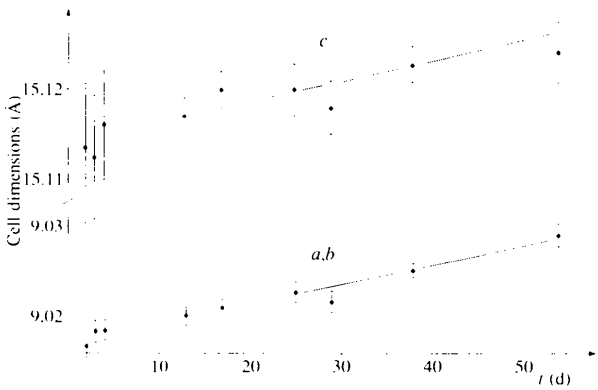

Fig. 4. $H_8Si_8O_{12}$. Cell dimensions at 9 K as a function of irradiation time. An inexpedient selection of centring reflections caused the relatively poorer values of standard deviations in the first few determinations for the c-axis length.

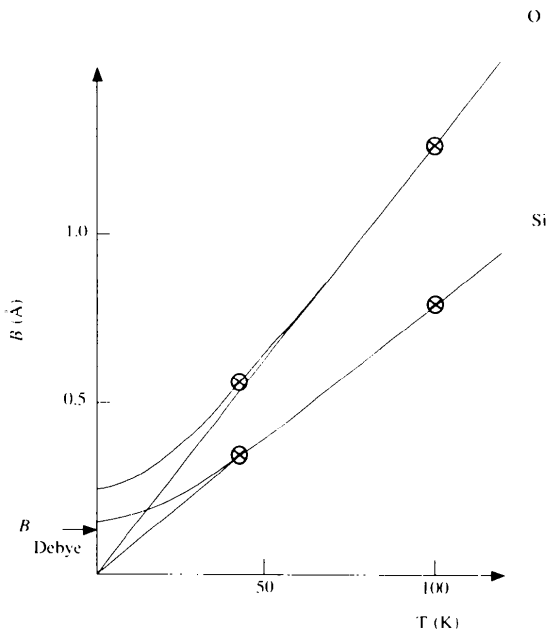

Fig. 5. $H_8Si_8O_{12}$. Equivalent isotropic temperature factor parameters. B_{Debye} indicates the lower limit for a zero-point value as calculated in the Debye approximation assuming a rigid-body molecule.

study are plotted at the nominal 100 K. It should also be remarked that the high-order data which strongly influence refinement values of the thermal parameters were collected mainly in the latter part of the data collection period, and so conceivably the values of B_{eq} will correspond well to the virtual temperature at the end of the experiment.

For a temperature of 9 K, the zero-point motion will lift the $B(T)$ curve above the line of proportionality with T. Therefore, it is not possible to predict an accurate value for the change in the isotropic temperature factor parameter of any early time during the data collection period. A lower limit for the zero-point value of the equivalent isotropic temperature factor parameter, $B_{Debye} = 0.13$ Å^2, can be calculated if the molecule is considered as a rigid body which behaves according to Debye theory (see Willis & Pryor, 1975). We can, for the sake of argument, assume the reduction to be half the value corresponding to the simple proportionality with T, *i.e.* $\Delta B = 0.5[B(100\,\text{K})/100]T$, and so for $T \simeq 10$ K we obtain $\Delta B \simeq 0.005$ Å^2 per degree. Since the change in effective temperature amounts to 0.64° per day, the change in isotropic thermal parameter is $\Delta B(t) \simeq 0.005 \times 0.64 = 0.003$ Å^2 per day. The time-dependent influence on intensities consequently will be $\exp[-2\Delta B(t)t\sin^2\theta/\lambda^2] = \exp(-0.012t\sin^2\theta)$ for t measured in d.

The radiation damage intensity loss for the four test reflections should manifest itself as a diffraction-angle-dependent decay in time. Two low-order reflections, (202) and ($\bar{2}22$), at $2\theta = 11.77°$, and two reflections at somewhat bigger diffraction angles, ($\bar{3}0\bar{9}$) at $2\theta = 29.20°$ and (648) at $2\theta = 52.14°$, were used as test reflections in the data collection. They were remeasured every 75 reflections. The two low-order test reflections hardly showed any continuous change over the data collection period, while the two higher-order reflections did indicate decay with time. The relative loss in intensity after 55 days amounted to approximately 5% for ($\bar{3}0\bar{9}$) and 15% for (648). This is, as expected, an indication that the scale factor calculated from the test reflections is both time- and diffraction-angle-dependent. The expression above for the intensity loss factor deduced from the radiation-damage-induced increase in cell dimensions and the observed reduction in thermal parameters predict 4% for ($\bar{3}0\bar{9}$) and 12% for (648), which conforms reasonably well with our observations.

The study of $H_8Si_8O_{12}$ has shown that radiation damage occurs even at 9 K and that it may be monitored by checking cell dimensions regularly during data collection, in addition to the usual repeated measurements of standard reflection intensity. For accurate studies, test reflections should be chosen at a selection of scattering angles, preferably some at rather high angles. Remembering the shape of the $B(T)$ curve, it is evident that the fall-off in intensity due to radiation damage will be slow in the beginning of the irradiation period and will pick up in speed until it reaches the state where ΔB becomes truely proportional to T. This observation gives yet another reason to recommend the lowest possible temperature for data collection.

6.2. $KTiO(PO_4)$: *a case of charge-density determination for a non-linear optical compound*

Solid-state laser device research is an area which has seen a rapid development lately. Enormous economic interests are at stake. Perfection of the blue–green laser technology based on the frequency-doubling capability of non-linear optical materials is a prerequisite for forging ahead the development of optical computers and storage media. Non-linear optical crystals are used in conjunction with III–V semiconductor IR lasers to generate light at half the wavelength of the diode. The bulk non-linear optical coefficients have been described (Levine, 1973) in a bond charge theory in terms of the combined effect of point bond charges residing in asymmetric potential wells. Chen (1986) has proposed calculating the overall second-harmonic generation by the geometrical superposition of perturbation of electrons by the incident radiation of anionic groups using a second-order perturbation theory.

Until now, only a small number of compounds have proved to be useful non-linear optical crystals. Potassium titanyl phosphate, $KTiOPO_4$ (KTP), has been recognized as the material of choice for second-harmonic generation because of a number of desirable physical properties: large non-linear optical coefficients, good optical transparency in the visible and near-IR regions, high power conversion efficiency and high threshold to laser-induced damage. The basic unit of the KTP structure is shown in Fig. 6. Many isomorphous derivations of the KTP structure have been synthesized, but only some of them show pronounced second-order non-linear optical effects. Stucky, Phillips & Gier (1989) have published a review on the extensive work in the KTP structure field. They conclude that non-linear susceptibility models concur that the microscopic hyperpolarizability of an octahedral metal centre increases with distortion of its geometry, and that the titanyl metal centre is primarily responsible for KTP's optical non-linearity.

Hansen, Protas & Marnier (1988, 1991) have performed an X-ray diffraction study of the detailed electron-density distribution of KTP for obtaining experimental insight into the polarization of the bonds of the structure. This is only possible with a highly accurate diffraction study. The relations between the crystal structure of KTP, the electron density around the titanium ions and the optical properties have been discussed by Hansen, Protas & Marnier (1988) and the detailed electron-density distribution in KTP at room temperature were subsequently published by the same authors (Hansen, Protas & Marnier, 1991). That study is an account of careful Ag $K\alpha$ X-ray diffraction measurements on single crystals. A multipolar analysis

was applied, and the study most convincingly indicated the presence of a strong covalent bond between Ti^{4+} and the O^{2-} ion. The non-linearity of KTP can be explained by the hyperpolarizability of the short Ti—O bonds in accordance with the idea that the hyperpolarizabilities are largest for polar covalent bonds. The P—O bonds of the phosphate groups do not seem to contribute to the high non-linear polarizability of KTP. The authors, however, were confronted with the difficulties presented by the non-centrosymmetry of the crystal structure. Because of the problem in accurately assigning phases to reflections in polar space groups, spurious features are more likely to appear than for structures of centrosymmetric space groups. For the KTP room-temperature study, the residual density around the K^+ ion for some models showed a pronounced non-spherical surrounding. Cations lie in relatively open channels along the *c* direction in the structure, and consequently KTP exhibits a moderately strong ionic conductivity. This may not have much direct influence on the optoelectronic properties, but it is a problem for detailed diffraction studies. Including non-spherical multipole functions at the K^+ site greatly reduced these features and did so more effectively than the introduction of an anharmonic Gram–Charlier expansion of the

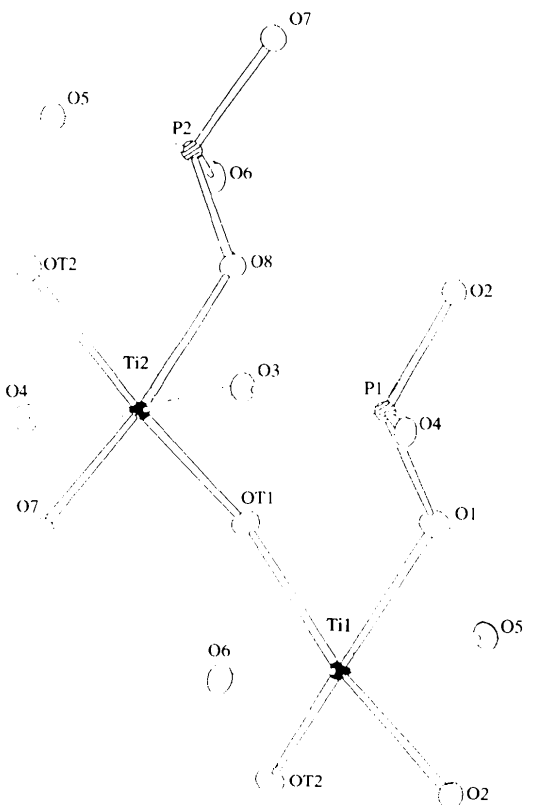

Fig. 6. $KTiOPO_4$. The basic unit of the structure showing the coordination around the Ti atoms. Average bond lengths: Ti—O = 1.98; short: Ti1—OT2 = 1.724, Ti2—OT1 = 1.745; long: Ti1—O1 = 2.150, Ti2—OT2 = 2.093 Å (e.s.d. $\simeq$ 0.001 Å).

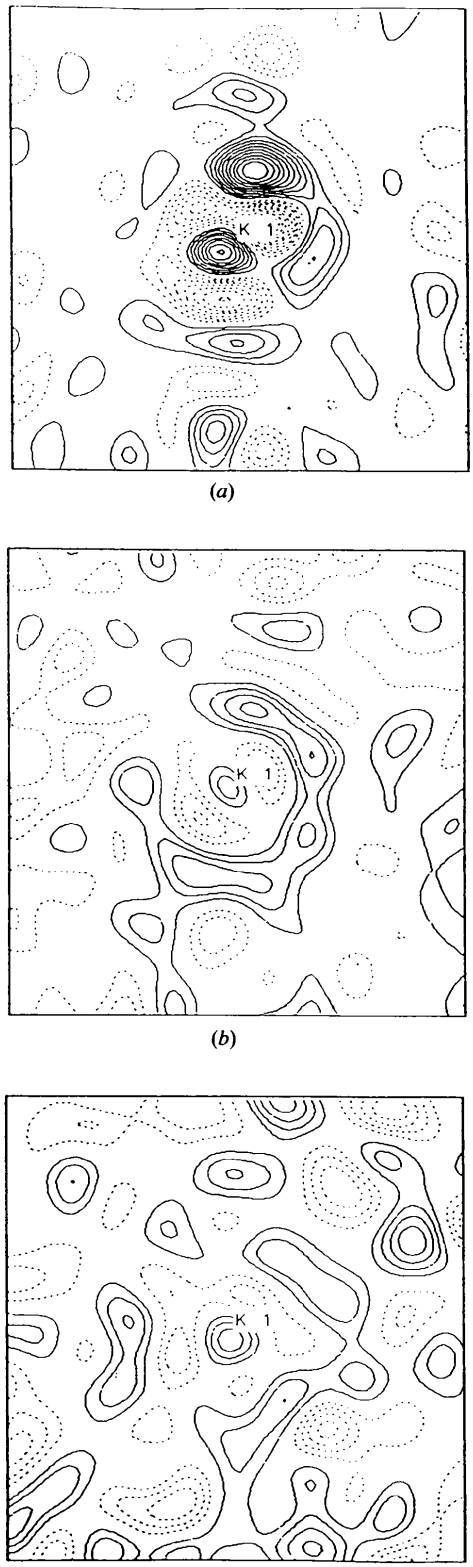

Fig. 7. $KTiOPO_4$. Residual density maps through the $K1^+$ ion for harmonic refinements. Interval between contours 0.1 e $Å^{-3}$ (*a*) room temperature, (*b*) 100 and (*c*) 9 K.

temperature factor. Modelling the density at the K^+ site influences the density near the titanium ions and it was thus deemed desirable to carry out a supplementary study at a temperature so low that anharmonic contributions to the atomic thermal motion can be safely considered insignificant.

A study based on Ag $K\alpha$ X-ray data collected at 9 K at Aarhus University has now been carried out in collaboration with the group from Nancy University. The structure apparently does not go through a phase transition during the cooling to 9 K. The potassium ions continue their shift along the c-axis direction, but their atomic displacement around the mean position is small at 9 K and can be described well in the harmonic approximation. This is also inferred from the maps of the residual density around the potassium ions. A set of maps for the K_1^+ ion at room temperature, 100 and 9 K, is shown in Fig. 7. It may be noted that the features near the K_1^+ ion become progressively smaller. In fact, the 9 K map is very similar to the room-temperature residual density map corresponding to a refinement using non-spherically symmetric density functions for K^+.

Static deformation-density maps are used to show redistributions of electrons caused by chemical bonding. They are defined as the difference between the total charge density calculated from the multipole parameters and the density of a model consisting of the sum of atomic contributions. Room-temperature static deformation density maps in the planes of the Ti atoms for this model are qualitatively very similar to the corresponding 9 K maps, which are shown in Fig. 8. Features at 9 K reach slightly higher values. Fig. 8(a) includes the short Ti—O bonds, and Fig. 8(b) shows the maps drawn perpendicular to those of Fig. 8(a). The deformation density in the phosphate groups is almost identical at the two temperatures. The conclusion in the case of KTP is that for this rather hard material the results of the room-temperature study with regard to the surroundings

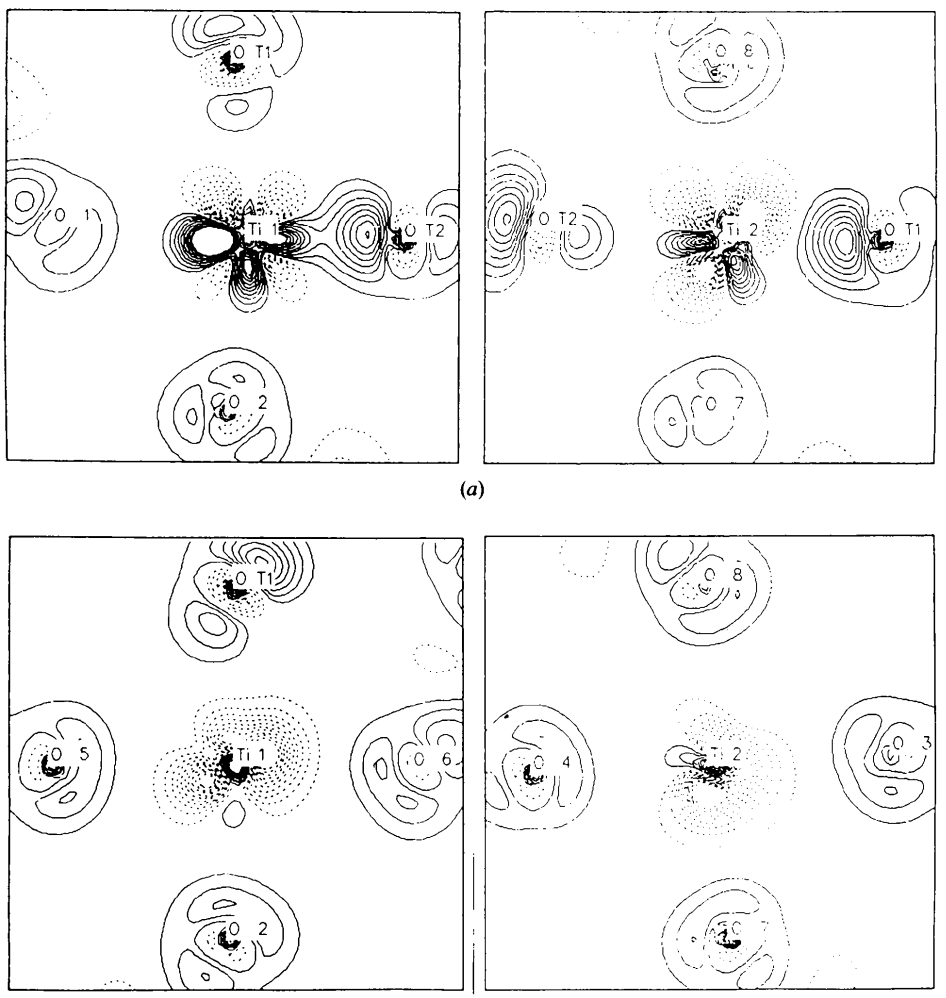

Fig. 8. $KTiOPO_4$. Static deformation-density maps from 9 K data, (a) including and (b) perpendicular to the short Ti—O bonds (Ti1—OT2 and Ti2—OT1). Interval between contours 0.1 e Å^{-3}.

of Ti were described correctly only by introducing an aspherical description of the K^+ density. The low-temperature study has provided improved knowledge of the electron density around K^+ and has given slightly more detailed information on the Ti—O bonds. In this case not much new information has been gained by the low-temperature experiment, but nagging suspicions that crucial results of the room-temperature studies, namely that the densities in the short Ti—O bonds were not correct, have been effectively removed and thus helped substantiate that the non-linearity of KTP can be explained by the hyperpolarizability of the short Ti—O bond.

Ultimately, the goal of the study is to probe the distribution and polarization of the electron density as a function of an applied field. This type of study has been carried out successfully in a few cases (Ståhl, Kvick & Abrahams, 1990; Graafsma *et al.*, 1992). Such studies have clearly shown that in spite of strong macroscopic physical effects, the shifts in atomic positions caused by an applied field are astonishingly small and diffraction studies must be of the highest precision in order to show the changes in the structure. This means that extended data sets have to be measured with great care taken to avoid systematic errors. It seems essential to opt for low-temperature studies in spite of the added complexity. For KTP, suspicion of an anharmonic motion of the K^+ ion at room temperature which seemed to influence the results of the density maps also near the crucial short Ti—O bonds made the low-temperature study imperative.

6.3. $(ND_4)_2Cu(SO_4)_2.6D_2O$: *A case of a combined X/N diffraction study of a Jahn–Teller distorted copper complex*

Many facets of the rich chemistry of 3*d* series transition-metal compounds have been explored by electron-density studies. Thus, the diammonium hexa-aquametal(II) disulfates, the Tutton salts, are excellent compounds for the study of metal–water bonding. The copper complex, especially, has attracted considerable attention. This is because the CuO_6 chromophore, pictured in Fig. 9, shows a strong Jahn–Teller distortion. Cu^{2+} has nine 3*d* electrons. The low-energy t_{2g} group of $3d_{xy}$, $3d_{xz}$ and $3d_{yz}$ orbitals are filled with three pairs of electrons and $3d_{z^2}$ of the higher energy e_g group of orbitals is also filled with a pair of electrons, while the $3d_{x^2-y^2}$ orbital is only half populated. This explains the Jahn–Teller effect. The uneven population of the e_g orbitals impedes the approach of ligands towards the Cu^{2+} ion along the *z* direction to as close a distance as the ligands approaching along the *x* and *y* directions.

The Cu^{2+} ion is located on a centre of inversion and for the $(NH_4)_2Cu(SO_4)_2.6H_2O$ compound at 293 K (Maslen, Watson & Moore, 1988), Cu—O7 = 2.228 (2), Cu—O8 = 2.078 (2) and Cu—O9 = 1.968 (2) Å. One pair of ligands has a longer distance than the two other pairs, but the geometry of the Cu—O6 chromophore changes considerably with temperature. This was interpreted (Alcock *et al.*, 1984) to be the result of a fluxional occupation of the three possible orientations of the long axis, so that at a particular temperature the observed structure will be an average of the three orientations weighted according to their relative thermal populations. The delicate balance in the copper Tutton salt structure also results in an interesting isotope effect (Hathaway & Hewat, 1984) of the copper–water system. Deuteration of the compound leads to a switch in the position of the long axis of the distorted $Cu(D_2O)_6^{2+}$ octahedron giving the distances: Cu—O7 = 2.081 (6), Cu—O8 = 2.242 (7) and Cu—O9 = 1.927 (6) Å. Very recently it has been shown that the switch to Cu—O7, again being the long axis as for the hydrogen-containing compound, may be triggered by increasing the hydrostatic pressure on the deuterated sample (Simmons, Hitchman, Stratemeier & Schultz, 1993). It has been a challenge to disentangle the many effects and reach a convincing electron-density distribution. This goal was achieved through a series of diffraction studies, both X-ray and neutron, at a number of temperatures.

The fact that the direction of the long axis shifts 90° by introducing deuterium instead of hydrogen or merely increasing the hydrostatic pressure on the deuterated sample suggests that some atoms sit in shallow energy minima. We (Iversen, Larsen, Reynolds & Figgis, 1994) have analysed the atomic thermal motion of the deuterated form for anharmonic behaviour from sets of neutron data collected at room temperature and at 15 K at the Danish Research Establishment Risø. The major difference between the switched structures is a change in hydrogen bonding between the ammonium ion hydrogen D13 to either O3 or O4, the two O atoms of the sulfate group. This part of the structure is shown in Fig. 10. The change of hydrogen bonding is accompanied by a slight rotation of the ammonium

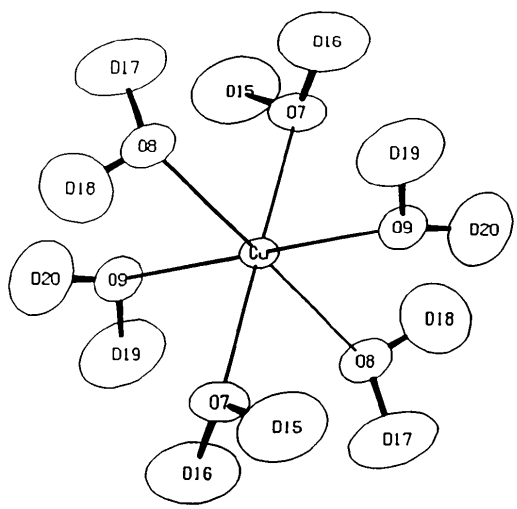

Fig. 9. $(ND_4)_2Cu(SO_4)_2.6D_2O$. The $Cu(D_2O)_6$ chromophore at 15 K with atoms shown as 50% probability ellipsoids.

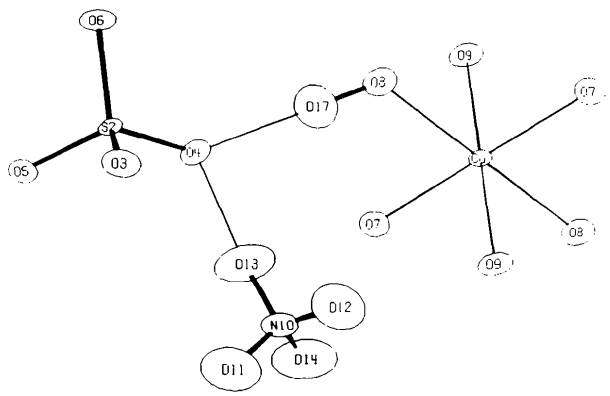

Fig. 10. $(ND_4)_2Cu(SO_4)_2.6D_2O$. The ammonium group, the sulfate group and the $Cu(D_2O)_6$ octahedron at 15 K with hydrogen bonds important for the position of the Jahn–Teller prolonged Cu—O distance. Atoms are shown as 50% probability ellipsoids.

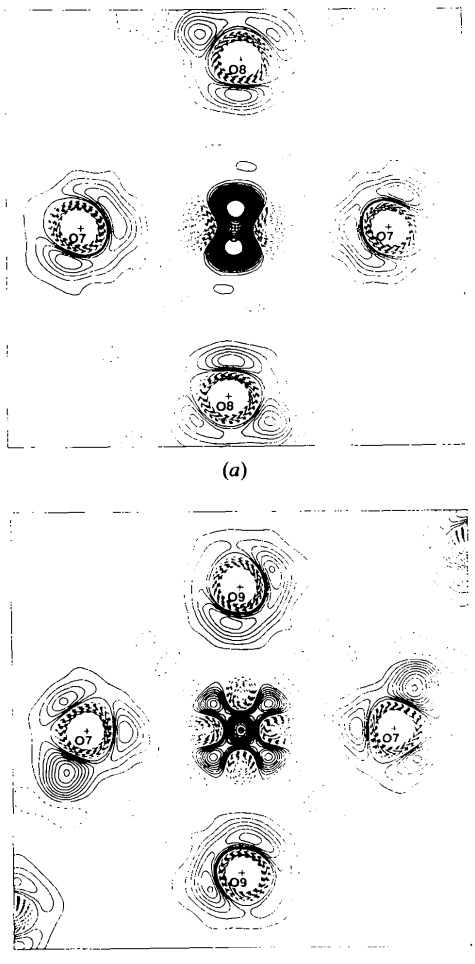

Fig. 11. $(ND_4)_2Cu(SO_4)_2.6D_2O$. Static deformation density (*a*) in the Cu—O7—O8 plane containing the Jahn–Teller prolonged Cu—O8 distance and (*b*) in the Cu—O7—O9 plane with the two short distances Cu—O7 and Cu—O9. Contour interval is 0.1 e Å^{-3}.

group. All the atoms of the ammonium group and the O3 and O4 atoms show significant anharmonic motion at room temperature – possibly as a kind of precursor for the switch. Only one other atom of the structure showed significant anharmonic motion at room temperature and only just. This is yet another example of how careful examination of thermal parameters can give information on incipient reaction pathways. The 15 K data showed no significant anharmonic contribution to the thermal motion. This we took as an indication that the structure at this temperature is in a minimum energy conformation for which it is possible to extract an accurate electron-density distribution.

6.3.1. *X/N modelling.* A multipole model was used in the refinement of the 9 K X-ray data measured at Aarhus University (Figgis *et al.*, 1993) and the availability of neutron data of an almost matching temperature of 15 K inspired the use of extra flexibility in the diffuse-density radial functions centred on the N, O and S atoms. When it was observed that high- and low-angle refinements of the X-ray data gave thermal parameters identical to the values found in the neutron diffraction study for Cu and S but not for O and N, model functions were added which can transfer density from more diffuse regions to those closer to the nucleus for the latter atom. Deuterium nuclear positions determined by the neutron diffraction experiment were kept fixed for consistency in the X-ray refinements. This required flexibility in the model for the D atoms, thus two Slater-type orbital 1*s* distributions were employed on each D atom with exponents of 1.0 and 0.5. Refinements with this model gave a very good fit, and very good consistency with the neutron structural results was achieved at the same time. Comparison of X-ray and neutron positional parameters showed no significant differences. For thermal parameters the mean difference between the two experiments was only 0.0003 Å^2.

The static deformation density was calculated. It was estimated to have standard deviations as modest as $\sim$ 0.04 e Å^{-3}. Two maps through the CuO_4 planes of the CuO_6 chromophore are presented in Fig. 11. The water molecules surrounding the Cu^{2+} ion show lone-pair density on the side towards Cu^{2+}. The maps may be interpreted to show the deficiency of density in the $3d_{x^2-y^2}$ orbital relative to that of $3d_{z^2}$. Cu—O8 is the distance prolonged by the Jahn–Teller effect and so presumably corresponds to the *z* direction of the Cu^{2+} local orbital Cartesian system. The surplus of density on Cu^{2+} indicates charge flow from the sulfate ion through water molecules to the Cu atom and, furthermore, Fig. 11(*a*) shows prolongation of the surplus density peak extending along the long Cu—O8 direction. The map in the plane of the short Cu—O bonds, Fig. 11(*b*), clearly shows the electron deficiency in the $3d_{x^2-y^2}$ orbitals as negative peaks in the direction towards the neighbouring water molecules. This picture of the distribution of

Table 1. $(ND_4)_2Cu(SO_4)_2.6D_2O$. *Valence-function populations at the Cu site; theoretical calculations are by Chandler, Christos, Figgis & Reynolds* (1992)

	9 K	Theory
$3d_{xy}$	2.14 (2)	1.95
$3d_{xz}$	2.02 (2)	1.96
$3d_{yz}$	2.01 (2)	1.96
$3d_{x^2-y^2}$	1.26 (2)	1.23
$3d_{z^2}$	2.07 (2)	1.98

$3d$ electrons also manifests itself in the numbers for the valence function populations at the Cu site. Table 1 shows experimental values which correspond quite well with results of theoretical calculations (Chandler, Christos, Figgis & Reynolds, 1992).

Copper Tutton salt has also been the subject of electron-density studies at room temperature (Maslen, Watson & Moore, 1988) and at 85 K (Figgis, Khor, Kucharski & Reynolds, 1992). Relative to these studies, the present one has had important gains from the use of very low temperatures in substantial reduction of anharmonicity and thermal diffuse scattering. The availability of results from a parallel neutron diffraction study allowed improvement of the multipole model by the introduction of extra flexible radial functions. The static deformation-density maps for the water molecule, the ammonium and the sulfate groups are all full of details which are now being compared with extended *ab initio* theoretical deformation-density maps. There is a very good qualitative, almost quantitative, correspondence between experiment and the present calculations, but further theoretical work is in progress. For the water molecules, Fig. 12, the main features are: A very deep hole at the O-atom nucleus, bonding density reaching 0.9 experimentally and 0.7 e $Å^{-3}$ in theory. Beyond the D atom a shallow hole of *ca* 0.1 e $Å^{-3}$, and behind the O-atom lone-pair densities of 0.4 and 0.5 e $Å^{-3}$, respectively, for experiment and theory. Equally good comparisons can be made for the ammonium ion, Fig. 13, but not quite for the sulfate ion, Fig. 14. The double peak in the S—O bonding density may be an artefact of modelling, but the feature of a rather flat maximum around the sulfur is most likely real and is yet clearly different from theory.

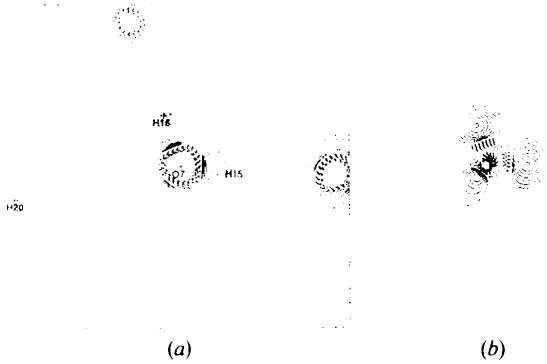

(*a*) (*b*)

Fig. 12. $(ND_4)_2Cu(SO_4)_2.6D_2O$. (*a*) Experiment, static deformation density in the plane of the water molecule O7—D15—D16 and (*b*) *ab initio* theoretical deformation density for the water molecule. Contours as in Fig. 11.

7. Concluding remarks

It has been shown that low-temperature diffraction studies of compounds with atoms as heavy as $3d$ series transition metals can provide very detailed information on geometry, atomic thermal motion and electron-density distributions challenging to theoretical physicists and chemists. In the near future with the advent of improved X-ray sources, in particular powerful, stable, dedicated X-ray synchrotron facilities, and with better detector systems, diffraction studies will undoubtedly be successfully carried out for compounds also containing heavier atoms. In spite of all the technical improvement it will still be prudent, if not indispensible, to collect data at the lowest possible temperature and further development of small light-weight cryocoolers, which can be fitted on standard diffractometers, would be most desirable.

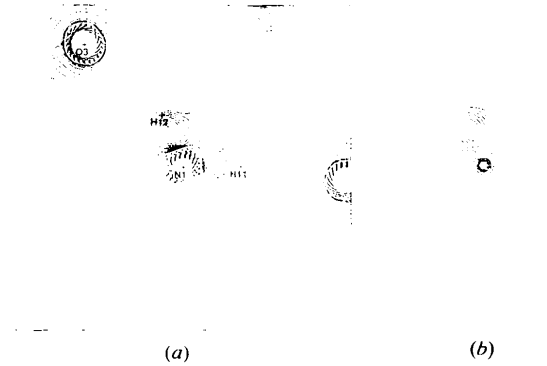

(*a*) (*b*)

Fig. 13. $(ND_4)_2Cu(SO_4)_2.6D_2O$. (*a*) Experiment, static deformation density in the N—D1—D2 plane of the ammonium ion and (*b*) *ab initio* theoretical deformation density in a similar plane for the ammonium ion. Contours as in Fig. 11.

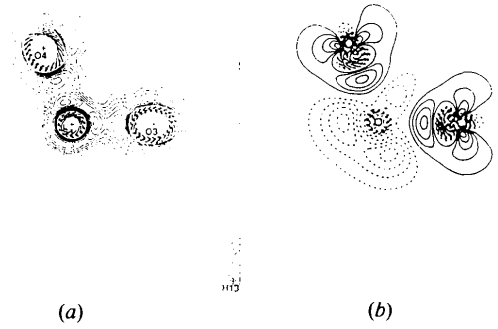

(*a*) (*b*)

Fig. 14. $(ND_4)_2Cu(SO_4)_2.6D_2O$. (*a*) Experiment, static deformation density in the S—O3—O4 plane of the sulfate ion and (*b*) *ab initio* theoretical deformation density in a similar plane as for the sulfate ion. Contours as in Fig. 11.

References

ALBERTSSON, J., OSKARSSON, Å. & STÅHL, K. (1979). *J. Appl. Cryst.* **12**, 537–544.

ALCOCK, N. W., DUGGAN, M., MURRAY, A., TYAGI, S., HATHAWAY, B. J. & HEWAT, A. (1984). *J. Chem. Soc. Dalton Trans.* pp. 7–14.

ARCHER, J. M. & LEHMANN, M. S. (1986). *J. Appl. Cryst.* **19**, 456–458.

AUF DER HEYDE, P. E., BÜRGI, H.-B., BÜRGY, H. & TÖRNROOS, K. W. (1991). *Chimia*, **45**, 38–40.

BOHR, J. (1991). RISØ-R-585. Risø National Laboratory, Roskilde, Denmark.

BOUVERET, Y. & MEGTERT, S. (1989). *J. Phys. Fr.* **50**, 1649–1671.

CHANDLER, G. S., CHRISTOS, G. A., FIGGIS, B. N. & REYNOLDS, P. A. (1992). *J. Chem. Soc. Faraday Trans.* 2, **88**, 1961–1969.

CHEN, C.-T. (1986). *Ann. Rev. Mater. Sci.* **16**, 203–243.

COMÉS, R. (1977). In *Chemistry and Physics of One-Dimensional Metals*, edited by H. J. KELLER. New York: Plenum Press.

COPPENS, P. & VOS, A. (1971). *Acta Cryst.* B**27**, 146–158.

COPPENS, D. D., COPPENS, P., LI, R. & LEE, P. (1993). *J. Appl. Cryst.* **26**, 226–228.

COPPENS, P., PETRICEK, V., LEVENDIS, D., LARSEN, F. K., PATURLE, A., YAN, G. & LEGRAND, A. D. (1987). *Phys. Rev. Lett.* **59**, 1695–1697.

COPPENS, P., ROSS, F. K., BLESSING, R. H., COOPER, W. F., LARSEN, F. K., LEIPHOLDT, J. G. & REES, B. (1974). *J. Appl. Cryst.* **7**, 315–319.

DAROVSKY, A., BOLOTOVSKY, R. & COPPENS, P. (1994). *J. Appl. Cryst.* **27**, 1039–1040.

FERRARIS, J., COWAN, D. O., WALATKA JR, V. & PERLSTEIN, J. H. (1973). *J. Am. Chem. Soc.* **95**, 948–949.

FIGGIS, B. N., IVERSEN, B. B., LARSEN, F. K. & REYNOLDS, P. A. (1993). *Acta Cryst.* B**49**, 794–806.

FIGGIS, B. N., KHOR, L., KUCHARSKI, E. S. & REYNOLDS, P. A. (1992). *Acta Cryst.* B**48**, 144–151.

FILHOL, A. (1994). In *Organic Conductors: Fundamentals and Applications*, edited by J. P. FARGES. New York: Marcel Dekker Inc.

GRAAFSMA, H., PATURLE, A., WU, L., SHEU, H.-S., MAJEWSKI, J., POORTHUIS, G. & COPPENS, P. (1992). *Acta Cryst.* A**48**, 113–120.

HANSEN, N. K., PROTAS, J. & MARNIER, G. (1988). *C. R. Acad. Sci. Ser. B*, **307**, 475–478.

HANSEN, N. K., PROTAS, J. & MARNIER, G. (1991). *Acta Cryst.* B**47**, 660–672.

HATHAWAY, B. J. & HEWAT, A. W. (1984). *J. Solid State Chem.* **51**, 364–375.

HENRIKSEN, K., LARSEN, F. K. & RASMUSSEN, S. E. (1986). *J. Appl. Cryst.* **19**, 390–394.

HOPE, H. (1988). *Acta Cryst.* B**44**, 22–26.

HOPE, H., FROLOW, F., VON BÖHLEN, K., MAKOWSKI, I., KRATKY, C., HALFON, Y., DANZ, H., WEBSTER, P., BARTELS, K. S., WITTMANN, H. G. & YONATH, A. (1989). *Acta Cryst.* B**45**, 190–199.

IVERSEN, B. B., LARSEN, F. K., REYNOLDS, P. A. & FIGGIS, B. N. (1994). *Acta Chem. Scand.* **48**, 800–809.

KURIYAMA, T., HAKAMADA, R., NAKGOME, H., TOKAI, Y., SAHASHI, M., LI, R., YOSHIDA, O., MATSUMOTO, K. & HASHIMOTO, T. (1989). *Proc. Intl Conf. on Cryogenics and Refrigeration*, pp. 91–99. Beijing: International Academic Publishers.

LARSEN, F. K. (1991). In *The Application of Charge Density Research to Chemistry and Drug Design*, edited by G. A. JEFFREY & J. F. PINIELLA, NATO ASI Series, Series B, Physics, Vol. 250. New York: Plenum Press.

LEVINE, B. F. (1973). *Phys. Rev. B*, **7**, 2600–2626

LUGER, P. (1993). *Cryst. Res. Technol.* **28**, 767–794.

MASLEN, E. N., WATSON, K. J. & MOORE, F. H. (1988). *Acta Cryst.* B**44**, 102–107.

RUDMAN, R. (1976). *Low-Temperature X-ray Diffraction. Apparatus and Techniques*. New York: Plenum Press.

RUDMAN, R., HOPE, H., STEVENS, E. D. & PETSKO, G. A. (1977). *LTXRD* Tutorial, Asilomar, California. American Crystallographic Association publication.

SAHASHI, M., TOKAI, Y., KURIYAMA, T., NAKAGOME, H., LI, R., OGAWA, M. & HASHIMOTO, T. (1989). *Proc. Int. Conf. on Cryogenics and Refrigeration*, pp. 131–139. Beijing: International Academic Publishers.

SAMSON, S., GOLDISH, E. & DICK, C. J. (1980). *J. Appl. Cryst.* **13**, 425–432.

SEILER, P. (1992). In *Accurate Molecular Structures*, edited by A. DOMENICANO & I. HARGITTAI. Oxford Univ. Press.

SIMMONS, C. J., HITCHMAN, M. A., STRATEMEIER, H. & SCHULTZ, A. J. (1993). *J. Am. Chem. Soc.* **115**, 11304–11311.

STUCKY, G. D., PHILLIPS, M. L. F. & GIER, T. E. (1989). *Chem. Mater.* **1**, 492–509.

STÅHL, K., KVICK, Å. & ABRAHAMS, S. C. (1990). *Acta Cryst.* A**46**, 478–485.

VEITH, M. & FRANK, W. (1988). *Chem. Rev.* **88**, 81–92.

WILLIS, B. T. M. & PRYOR, A. W. (1975). In *Thermal Vibrations in Crystallography*. Cambridge Univ. Press.

ZEYEN, C. M. E., CHAGNON, R., DISDIER, F. & MORIN, H. (1984). *Rev. Phys. Appl.* **19**, 789–791.